



 Cite this: *RSC Adv.*, 2024, 14, 27935

# Antiviral activity of pyrazole derivatives bearing a hydroxyquinoline scaffold against SARS-CoV-2, HCoV-229E, MERS-CoV, and IBV propagation†

 Alaa R. I. Morsy,<sup>§a</sup> Sara H. Mahmoud,<sup>‡§b</sup> Noura M. Abou Shama,<sup>b</sup> Walaa Arafa,<sup>c</sup> Gehad A. Yousef,<sup>a</sup> Ahmed. A. Khalil<sup>\*d</sup> and Sayed K. Ramadan <sup>\*e</sup>

The ongoing global threat posed by coronaviruses necessitates the urgent development of effective antiviral agents. In this study, we investigated the potential of hydroxyquinoline-pyrazole candidates as antiviral agents against a range of coronaviruses, including SARS-CoV-2, MERS-CoV, and HCoV-229E. Molecular docking studies were conducted to assess the binding affinity of the synthesized compounds to key viral proteins. The compounds were prepared *via* condensation reactions of a pyrazolyhydrazide derivative with 2-chloro-3-formylquinoline, yielding hydrazone and pyrrolone derivatives. The cytotoxicity of compounds was evaluated using Vero E6 cells, and their antiviral activity was assessed *via* plaque reduction assays and viral inhibition assays using hydroxychloroquine as a positive control antiviral drug. The results revealed promising antiviral activity of the synthesized compounds against all tested coronaviruses, with selectivity indices indicating their potential as selective antiviral agents. Notably, the compounds exhibited potent inhibition of SARS-CoV-2 at lower concentrations, highlighting their promise as therapeutic candidates against this highly pathogenic virus. Likewise, the modeling pharmacokinetics approach showed its appropriate drug-likeness and bioavailability assets. These findings underscore the importance of hydroxyquinoline-pyrazole derivatives as potential antiviral agents against diverse coronaviruses, providing valuable insights for further therapeutic development.

 Received 29th June 2024  
 Accepted 27th August 2024

DOI: 10.1039/d4ra04728a

[rsc.li/rsc-advances](https://rsc.li/rsc-advances)

## Introduction

The Coronavirus (CoVs) family recently became well-known pathogens that can cause severe respiratory diseases with varying incidences around the globe. Among them, Severe Acute Respiratory Syndrome Coronavirus 2 (SARS-CoV-2) that causes COVID-19, has brought the world to the overwhelming pandemic level and caused significant socio-economic losses. While the novel coronavirus's outbreak has been somewhat curbed through vaccination and public health measures, the demand for successful antiviral medications is still relevant,

especially given the further appearance of new strains and likelihood of other zoonotic spills.<sup>1,2</sup>

Due to the emergence of the coronaviruses and subsequent severe acute respiratory syndrome (SARS) and Covid-19, the necessity of effective and potent antiviral agents targeting the viral proteins that are vital for the replication and pathogenesis of the virus has surged.<sup>3,4</sup> In this respect, heterocyclic compounds have attracted much interest because of the numerous biological activities and action they exhibit as antiviral substances.<sup>5,6</sup> Among these, the pyrazole moiety is known to be useful in drug design because it also provides several synthetic approaches and structural variations for the improvement of the pharmacological profile of the target drug.<sup>7-9</sup> Also, the representatives of hydroxyquinoline derivatives have become the object of interest because of their activity against a wide range of viruses, tumors, and suitable pharmacokinetic properties.<sup>10,11</sup>

New research studies have been carried out regarding the antiviral activity of hydroxyquinoline and pyrazole derivatives. For example, Saadeh *et al.* described the recent findings on the synthesis and biological activities of 8-hydroxyquinolines as antiviral agents with a wide spectrum.<sup>12</sup> Likewise, pyrazole derivatives are effective molecules in the fight against many viral diseases caused by viruses belonging to different families, including coronavirus. Seliem *et al.* synthesized

<sup>a</sup>Central Laboratory for Evaluation of Veterinary Biologics (CLEVB), Agricultural Research Center, Cairo, Egypt

<sup>b</sup>Center of Scientific Excellence for Influenza Viruses, National Research Centre (NRC), Egypt

<sup>c</sup>Microbiology Department, Faculty of Agriculture, Cairo University, Egypt

<sup>d</sup>Veterinary Sera and Vaccines Research Institute (VSVRI), Agricultural Research Center (ARC), Cairo, Egypt. E-mail: ahme\_2001@hotmail.com

<sup>e</sup>Chemistry Department, Faculty of Science, Ain Shams University, Cairo, 11566, Egypt. E-mail: sayed.karam2008@sci.asu.edu.eg

 † Electronic supplementary information (ESI) available. See DOI: <https://doi.org/10.1039/d4ra04728a>

§ Equal contributing first authors.

\* Current affiliation: Texas Biomedical Research Institute, Texas, USA.



pyrazolothiazole conjugates and screened them through virtual methods, and thus they showed that pyrazole class compounds have potential for hits on viral proteins of SARS-CoV-2.<sup>13</sup>

In addition, the incorporation of various heterocyclic fragments is a recent approach to the improvement of biological activity.<sup>14–16</sup> Kandinska *et al.* prepared tetrahydroisoquinoline derivatives containing other heterocycles and a comparative evaluation for anti-coronavirus activity was investigated.<sup>17</sup> This approach indicates the use of a variety of pharmacophores which is parallel to our concept of selecting both hydroxyquinoline and pyrazole core.

While several articles have been published on the pharmacological aspects of hydroxyquinoline-pyrazole derivatives, our work describes the first conceptual investigation on their antiviral profiles against coronaviruses: SARS-CoV-2 or Covid-19, MERS-CoV, and HCoV-229E. These compounds were characterized as antiviral based on the obtained SAR result from molecular modeling, synthetic and biological studies of the compounds and experiments to establish their mode of action.

Concerning the compound development and optimization of the identified leads, utilization of the computational tools based on structure–activity relationship in assist of compound optimization results in even improved antiviral efficacy and pharmacokinetic profile for further series of *in vitro* and *in vivo* studies. As a result of these findings, there are roles for a further study *in vivo* efficacy and toxicity in a further study in view of the modesty seen in this study. Also, it is possible to explore variations of the structure of the synthesized compounds to enhance their antiviral activity and selectivity.

Outcomes of the current research serve as the foundation for the other studies towards the investigation of the effective antiviral treatment towards coronaviruses, which is a key priority of today's healthcare systems. Thus, hydroxyquinoline-pyrazole derivatives can be regarded as a basis for the series of the new generation of multivalent antiviral agents in fighting against the new coronavirus and other similar viral infections in the future.

## Materials and methods

### Chemistry

Melting points were measured on a Gallenkamp electric melting point apparatus (SANYO GALENKAMP, UK) and are uncorrected. The reactions were monitored by thin-layer chromatography (TLC) using precoated Merck Kiesel gel 60F<sub>254</sub> aluminum backed plates obtained from Fluka, Switzerland. All reagents and solvents were purified and dried by standard techniques. The infrared spectra were recorded using potassium bromide disks on FTIR Thermo Electron Nicolet iS10 (USA) infrared spectrometer and expressed in wave number ( $\nu$ , cm<sup>-1</sup>) at Faculty of Science, Ain Shams University. The <sup>13</sup>C and <sup>1</sup>H NMR spectra were run at 100 and 400 MHz on a Bruker NMR spectrometer (Bruker, Manufacturing & Engineering Inc., Anaheim, CA, USA) using TMS as an internal standard in DMSO at Faculty of Pharmacy, Cairo University. Chemical shifts ( $\delta$ ) are quoted in ppm. Mass spectrum was carried out on direct probe controller inlet part to single quadrupole mass analyzer in

Thermo Scientific GCMS, MODEL ISQLT operating at 70 eV using Thermo X-Calibur software at the regional center for mycology and biotechnology (RCMB), Al-Azhar University, Cairo, Egypt. The starting pyrazolyldiazide derivative (**Hyd**) was previously reported.<sup>7</sup>

### Condensation of the hydrazide (**Hyd**) with 2-chloro-3-formylquinoline

A solution of the pyrazolyldiazide derivative (**Hyd**) (2.11 g, 5 mmol), 2-chloro-3-formylquinoline (0.95 g, 5 mmol) in 1,4-dioxane (20 mL) was refluxed for 30 min. The precipitated solid while heating was filtered off and recrystallized from 1,4-dioxane to produce the hydrazone derivative (**HQ**). When the reaction mixture was refluxed in an absolute ethyl alcohol (20 mL) including glacial acetic acid (0.1 mL) for 1 h, the precipitated solid while heating was filtered and recrystallized from ethanol/1,4-dioxane mixture (2:1) to afford the pyrrolone derivative (**15A**).

### 2-((1,3-Diphenyl-1H-pyrazol-4-yl)methylene)-N'-((2-hydroxyquinolin-3-yl)methylene)-4-oxo-4-phenylbutanehydrazide (**HQ**)<sup>8</sup>

Yellow crystals, mp. 330–332 °C [(ref. 8) mp. 330–332 °C], yield 77%. FTIR ( $\nu$ , cm<sup>-1</sup>): 3422 (OH), 3161 (NH), 3059, 3007 (CH-aromatic), 2954, 2895 (CH-aliphatic), 1669 (C=O), 1612 (C=N). <sup>1</sup>H NMR (400 MHz, DMSO-*d*<sub>6</sub>,  $\delta$ , ppm): 12.15 (br. s, 2H, OH + NH, exchangeable), 9.14 (s, 1H, CH=N), 8.90 (s, 1H, C<sub>5</sub>-H pyrazole), 8.83 (s, 1H, C<sub>4</sub>-H quinoline), 8.24–8.22 (d, 1H, C<sub>5</sub>-H quinoline, *J* = 8 Hz), 8.00–7.98 (m, 3H, quinoline-H), 7.87–7.36 (m, 15H, aryl-H), 7.22 (s, 1H, CH=), 3.54 (s, 2H, CH<sub>2</sub>). <sup>13</sup>C NMR (100 MHz, DMSO,  $\delta$ , ppm): 39.38 (CH<sub>2</sub>), 102.97, 104.53, 105.75, 107.48, 109.04, 110.60, 111.81, 112.51, 115.98, 118.92, 120.66, 123.26, 125.16, 126.72, 127.76, 130.19, 132.44, 133.14, 135.91, 137.99, 140.59, 142.50, 145.45, 147.70, 149.61 (C=N), 167.81 (N-C=O), 177.69 (N=C-OH), 196.76 (C=O ketone). EIMS (70 eV, *m/z*, %): 577.04 (M<sup>+</sup>, 26.93), 541.32 (40.14), 507.46 (54.70), 483.74 (44.54), 441.67 (43.34), 411.03 (61.81), 395.83 (51.65), 376.67 (43.89), 362.02 (71.87), 348.17 (37.34), 330.01 (52.15), 308.73 (75.58), 301.27 (56.86), 217.16 (51.15), 201.28 (32.73), 177.89 (53.35), 159.40 (53.10), 140.81 (40.89), 137.26 (100.00), 130.66 (95.25), 126.75 (51.75), 113.68 (38.19), 91.72 (63.36), 74.51 (59.51). Anal. calcd for C<sub>36</sub>H<sub>27</sub>N<sub>5</sub>O<sub>3</sub> (577.64): C, 74.86; H, 4.71; N, 12.12; found: C, 74.71; H, 4.60; N, 12.09%.

### 3-((1,3-Diphenyl-1H-pyrazol-4-yl)methylene)-1-(((2-hydroxyquinolin-3-yl)methylene)amino)-5-phenyl-1,3-dihydro-2H-pyrrol-2-one (**15A**)<sup>8</sup>

Orange crystals, mp. 237–239 °C [(ref. 8) mp. 237–239 °C], yield 80%. FTIR ( $\nu$ , cm<sup>-1</sup>): 3442 (OH), 3058 (CH-aromatic), 1699 (C=O), 1617 (C=N). <sup>1</sup>H NMR (400 MHz, DMSO-*d*<sub>6</sub>,  $\delta$ , ppm): 12.13 (s, 1H, OH, exchangeable), 9.33 (s, 1H, CH=N), 9.25 (s, 1H, C<sub>5</sub>-H pyrazole), 8.89 (s, 1H, C<sub>4</sub>-H quinoline), 8.08–8.06 (d, 1H, C<sub>5</sub>-H quinoline, *J* = 8 Hz), 7.96–7.82 (m, 3H, quinoline-H), 7.75–7.38 (m, 15H, aryl-H), 7.23 (s, 1H, CH=), 7.00 (s, 1H, C<sub>4</sub>-H pyrrole). <sup>13</sup>C NMR (100 MHz, DMSO,  $\delta$ , ppm): 100.78, 105.92, 108.72, 113.37, 115.38, 117.13, 119.51, 119.84, 121.92, 124.60, 126.47,



127.75, 128.74, 128.85, 128.91, 129.16, 129.31, 129.40, 130.04, 132.30, 139.43, 142.94, 145.74, 149.47, 151.46, 167.64 (C=O), 177.69 (N=C-OH). EIMS (70 eV,  $m/z$ , %): 559.91 ( $M^+$ , 49.94), 556.79 (28.44), 548.86 (32.66), 544.26 (48.26), 541.51 (61.02), 534.86 (41.66), 512.23 (33.42), 500.07 (28.63), 486.94 (66.73), 481.86 (67.08), 474.31 (73.97), 469.29 (55.88), 459.23 (55.88), 452.99 (66.46), 447.17 (54.70), 436.17 (98.43), 416.88 (100.00), 406.74 (69.07), 391.52 (31.81), 378.58 (50.90), 367.16 (37.98), 365.82 (40.78), 353.80 (56.42), 347.06 (49.75), 330.68 (35.30), 322.21 (28.36). Anal. calcd for  $C_{36}H_{25}N_5O_2$  (559.63): C, 77.26; H, 4.50; N, 12.51; found: C, 77.14; H, 4.38; N, 12.53%.

### ADME analysis

The absorption, distribution, metabolism, and excretion (ADME) properties of the synthesized compounds were evaluated using the SwissADME web tool (<http://www.swissadme.ch>). This free online platform allows for the prediction of physicochemical properties, lipophilicity, water solubility, pharmacokinetics, drug-likeness, and medicinal chemistry friendliness of small molecules. The following key parameters were assessed:

(1) Physicochemical properties: molecular weight, number of heavy atoms, number of aromatic heavy atoms, fraction of carbons in  $sp^3$  hybridization, number of rotatable bonds, number of H-bond acceptors and donors, molar refractivity, and topological polar surface area (TPSA).

(2) Lipophilicity: consensus  $\log P_{ow}$  was calculated using five predictive models (XLOGP3, WLOGP, MLOGP, SILICOS-IT, and iLOGP).

(3) Water solubility:  $\log S$  values were predicted using three models (ESOL, Ali, and SILICOS-IT).

(4) Pharmacokinetics: gastrointestinal (GI) absorption, blood-brain barrier (BBB) permeation, P-glycoprotein substrate, and interaction with cytochrome P450 isoenzymes (CYP1A2, CYP2C19, CYP2C9, CYP2D6, CYP3A4) were evaluated.

(5) Drug-likeness: compliance with Lipinski's rule of five, Ghose, Veber, Egan, and Muegge rules was assessed.

(6) Medicinal chemistry: PAINS (Pan-Assay Interference Compounds) and Brenk alerts, along with lead-likeness were determined.

The results were interpreted using the BOILED-Egg model, which provides a graphical representation of the compounds' gastrointestinal absorption and brain penetration. Additionally, the bioavailability radar chart was used to assess the drug-likeness of the compounds based on six physicochemical properties: lipophilicity (LIPO), size, polarity (POLAR), solubility (INSOLU), flexibility (FLEX), and saturation (INSATU).

The significance of these parameters lies in their ability to predict the compounds' behavior in biological systems, their potential as drug candidates, and their likelihood of success in

further development stages. This analysis provides crucial information for prioritizing compounds and guiding future optimization efforts in the drug discovery process.

## Molecular modeling studies

### Molecular docking study

Molecular docking studies of the compounds were performed using Molecular Operating Environment software. All minimizations were carried out until an RMSD gradient of  $0.05 \text{ kcal mol}^{-1} \text{ \AA}^{-2}$  with MMFF94x force field and the partial charges were automatically calculated. The structure of Proteins was downloaded from the Protein Data Bank. For docking study, the protein was prepared by Protonate 3D protocol with default options and water molecules removal. The co-crystallized ligand was used to determine the active site for docking. London dG and Triangle Matcher placement scoring function were used for docking study.

## In vitro methods

### Viruses and cells

The SARS-CoV-2 strain (GISAID number: EPI\_ISL\_430819)<sup>18</sup> from the CoV-19/Egypt/NRC-03/2020, the MERS-CoV strain NRCE-HKU270 (Genbank accession: KJ477103.2),<sup>19</sup> and HCoV-229E were cultured and amplified in Vero E6 cells (ATCC CRL-1587) until the observation of cytopathic effects (CPE).<sup>20</sup> The Vero E6 cells were obtained from American Type Culture Collection (ATCC). Subsequently, the viruses were quantified using TCID50 (50% tissue culture infectious dose), following established protocols.<sup>21,22</sup> Hydroxychloroquine was used as a positive control antiviral drug.

### Cytotoxicity determination ( $CC_{50}$ )

Three synthetic compounds were dissolved in dimethyl sulfoxide (DMSO, Sigma-Aldrich) at a concentration of  $10 \text{ mg mL}^{-1}$ . Cytotoxic activity was tested in Vero-E6 cells using a crystal violet assay as previously described<sup>22</sup> with minor modifications. Briefly, the cells were seeded in 96-well plates ( $100 \mu\text{L}$  per well at a density of  $3 \times 10^5$  cells per mL) and incubated for 24 h at  $37^\circ\text{C}$  in 5%  $\text{CO}_2$ . After 24 h, the cells were treated with various concentrations of the compound in triplicate. At 72 h post-treatment, the supernatant was discarded, and cell monolayers were fixed with 10% formaldehyde for 1 h at room temperature (RT). The fixed monolayers were then dried thoroughly and stained with  $50 \mu\text{L}$  of 0.1% crystal violet for 20 min on a bench rocker at room temperature. The monolayers were then washed, dried overnight, and the crystal violet dye in each well was dissolved in  $200 \mu\text{L}$  methanol for 20 min on a bench rocker at room temperature. The absorbance of the crystal violet

$$\text{Cytotoxicity}\% = \frac{\text{absorbance of cells without treatment} - \text{absorbance of cells with treatment}}{\text{absorbance of cells without treatment}} \times 100$$



solutions was measured at  $\lambda_{\text{max}}$  570 nm as a reference wavelength using a multi-well plate reader. The  $\text{CC}_{50}$  value was calculated using nonlinear regression analysis using GraphPad Prism software (version 5.01) by plotting log concentrations of the compound *versus* normalized response (variable slope).

The concentration that displayed 50% cytotoxicity ( $\text{CC}_{50}$ ) was calculated using a plot of percent cytotoxicity *versus* sample concentration.<sup>23</sup>

### Inhibitory concentration determination ( $\text{IC}_{50}$ )

The  $\text{IC}_{50}$  values for the compounds were determined as previously described,<sup>24</sup> with slight modifications.  $2.4 \times 10^4$  Vero-E6 cells were placed in each well of 96-well tissue culture plates and cultured overnight at 37 °C in a humidified 5%  $\text{CO}_2$  incubator. After that, the cell monolayers were rinsed once in  $1 \times$  PBS. An aliquot of the SARS-CoV-2, MERS-CoV and HCoV-229E viruses<sup>25</sup> containing 100  $\text{TCID}_{50}$  were incubated with serially diluted concentrations of the tested compound and kept at 37 °C for 1 h. Another set of Vero-E6 cells were treated with virus/compound mix and co-incubated at 37 °C in a total volume of 200  $\mu\text{L}$  per well. Untreated cells infected with a virus represent virus control; however, cells that have not been treated and have not been infected represent cell control. The cells were fixed with 100  $\mu\text{L}$  of 10% paraformaldehyde for 20 min and stained with 0.5% crystal violet in distilled water for 15 min at room temperature after being incubated for 72 h at 37 °C in a 5%  $\text{CO}_2$  incubator. After that, 100  $\mu\text{L}$  absolute methanol per well was used to dissolve the crystal violet dye and the optical density of the color was measured at 570 nm using Anthos Zenyth 200rt plate reader (Anthos Labtec Instruments, Heerhugowaard, Netherlands). The  $\text{IC}_{50}$  of a compound is required to reduce the virus-induced cytopathic effect (CPE) by 50%, relative to the virus control. The  $\text{IC}_{50}$  value was calculated using nonlinear regression analysis of GraphPad Prism software (version 5.01) by plotting log concentrations of the compounds *versus* normalized response (variable slope).

### *In vitro* mechanism of virus inhibition

The antiviral activity of the three synthesized compounds (hydrazide **Hyd**, hydrazone **HQ**, and pyrrolone **15A**) was evaluated against SARS-CoV-2, MERS-CoV, and HCoV-229E using dose-dependent viral inhibition assays. These assays were conducted following previously established methods, with minor modifications to optimize for our specific experimental conditions.<sup>25</sup>

### Viral replication

Viral replication inhibition was assessed to determine the compound's ability to interfere with the coronavirus life cycle within host cells, viral dilutions of SARS-CoV-2 virus were allowed to infect Vero-E6 cells cultured at a density of  $1.2 \times 10^6$  cells per well in a 6-well plate for 24 h. Each plate contains cell and virus control wells to ensure the validity of the assay and to calculate the percent of viral inhibition following treatment, respectively. The plates were incubated at 37 °C in a humidified

5%  $\text{CO}_2$  incubator for 1 h. Cell monolayers were then washed with  $1 \times$  PBS. Subsequently, the different predetermined non-cytotoxic concentrations of each compound were applied, and the plates underwent a second incubation period at 37 °C in a humidified 5%  $\text{CO}_2$  incubator for 1 h. Cells were washed again and the 2% agarose overlayers were added then the plates were incubated at 37 °C in a humidified 5%  $\text{CO}_2$  incubator for 72 h. The cell monolayers were then fixed and stained using 0.1% crystal violet solution as described previously in the plaque infectivity assay.<sup>26</sup>

### Viral adsorption

A range of non-cytotoxic concentrations were applied to the precultured Vero-E6 cells in 6 well plates ( $1.2 \times 10^6$  cells per well). Each plate contains cell and virus control wells to ensure the validity of the assay and to calculate the percent of viral inhibition following treatment, respectively. The plates were then incubated at 4 °C for 1 h to allow chemical adsorption onto cell receptors without active penetration. The plates were then washed with  $1 \times$  PBS to remove the residual compounds. Subsequently, the countable viral dilution of SARS-CoV-2 virus was applied to allow viral adsorption/infection and another incubation period was employed at 37 °C in a humidified 5%  $\text{CO}_2$  incubator for 1 h. The cell monolayers were then washed with  $1 \times$  PBS to remove the residual virus and overlaid with 2% agarose/2X DMEM overlay and incubated at 37 °C in a humidified 5%  $\text{CO}_2$  incubator for 72 h. The cell monolayers were then fixed and stained using 0.1% crystal violet solution as described previously in the plaque infectivity assay.<sup>27</sup>

### Virucidal effect

A simple plaque reduction assay was performed where effective concentrations of the compounds were mixed with concentrated SARS-CoV-2 virus (3–4 folds higher than the countable virus dilution). The virus/compound mixture was then incubated at room temperature for 1 h. Subsequently, ten-fold serial dilutions of the virus/compound mixture (3 or 4 times) were performed to reach a countable viral titer. The mixture dilution with countable viral titer was then applied to the Vero-E6 monolayers ( $1.2 \times 10^6$  cells per well) including cell and virus control wells. The plates were then incubated at 37 °C in a humidified 5%  $\text{CO}_2$  incubator for 1 h. To remove the remains of the mixture, cell monolayers were washed with  $1 \times$  PBS and overlaid with 2% agarose/2X DMEM, and incubated at 37 °C in a humidified 5%  $\text{CO}_2$  incubator for 72 h. The cell monolayers were then fixed and stained, visualized using 0.1% crystal violet solution as described previously in the plaque infectivity assay.<sup>28</sup>

## Results

### Compounds' synthesis

Our research was concerned with the design and construction of a wide variety of nitrogen containing heterocycles exhibiting synthetic and pharmacological importance. Noteworthy, pyrazoles have been reported as a new scaffold of good antiviral agents.<sup>8,29,30</sup> Likewise, quinolines have attracted a tremendous



attention due to their existence in some of well-known drugs.<sup>30–32</sup> This broad spectrum of biological properties initiated our interest to examine the heterocyclic systems gathering pyrazole and quinoline scaffolds in one skeleton.

Thus, the readily obtainable acid hydrazide **Hyd**<sup>7</sup> was condensed with 2-chloro-3-formylquinoline under two different reaction media to produce the hydrazone **HQ** and pyrrolone **15A** candidates encompassing each of pyrazole and quinoline scaffolds in spectacular yields (Fig. 1).<sup>8</sup> Initially, refluxing of an equimolar mixture of pyrazolyhydrazide **Hyd** and the former quinoline aldehyde in 1,4-dioxane as a solvent afforded the corresponding hydrazone derivative **HQ**. On the other hand, when the reaction was executed in boiling ethanol containing glacial acetic acid, the pyrrolone derivative **15A** was obtained as a sole product.

The chemical structures of all products were based on their analytical and spectroscopic data. The IR spectrum of quinolinylhydrazone **HQ** exhibited the characteristic stretching absorption bands for OH, NH, C=O and C=N groups at  $\nu$  3422, 3161, 1669, and 1612  $\text{cm}^{-1}$ , respectively. The <sup>1</sup>H NMR spectrum of hydrazone **HQ** showed singlet signals for NH and CH<sub>2</sub> protons which disappeared in that of pyrrolone **15A**. Compelling evidence for the structures of compounds **HQ** and **15A** were acquired from their <sup>13</sup>C NMR spectra which provided the characteristic signals to these structures. Furthermore, their mass spectra exhibited the molecular ion peaks and some important abundant peaks.

Formation of hydrazone **HQ** could be visualized to occur *via* elimination of water molecule followed by removal of chlorine under heating conditions. The formation of pyrrolone **15A** could be explained *via* ring closure of hydrazone **HQ**. This behavior was interpreted *via* acid catalyzed 1,5-*exo*-trig cyclization. These compounds were evaluated for their antiviral activity and displayed promising potency as *vide supra* (100% protection against Newcastle Disease Virus).<sup>8</sup>

### In silico molecular docking results

In the present study, four proteins were used for docking simulation, as follows: (i) PDB ID: 7YRZ which is the crystal structure of HCoV 229E main protease in complex with

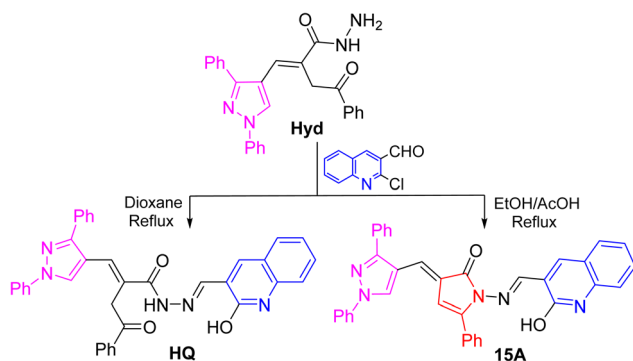


Fig. 1 Synthesis of target antiviral agents, pyrazole-based quinoline derivatives (pyrazolyhydrazide **Hyd**, hydrazone **HQ**, and pyrrolone **15A**).

PF07321332 (Nirmatrelvir is an antiviral drug that acts as an orally active 3C-like protease inhibitor), (ii) PDB ID: 2Q6F which is the crystal structure of infectious bronchitis virus (IBV) main protease in complex with a Michael acceptor inhibitor N3 (the coronavirus main protease (M(pro)), which plays a pivotal role in viral gene expression and replication through the proteolytic processing of replicase polyproteins), (iii) PDB ID: 6VGY which is the 2.05 Å resolution structure of MERS 3CL protease in complex with inhibitor 6b (hydrolase inhibitor), (iv) PDB ID: 6WUU which is the crystal structure of the SARS CoV-2 papain-like protease in complex with peptide inhibitor VIR250 (viral papain-like cysteine protease (PLpro, NSP3) is essential for SARS-CoV-2 replication and represents a promising target for the development of antiviral drugs). These proteins are used as a target to test the compounds (hydrazide **Hyd**, hydrazone **HQ**, and pyrrolone **15A**).

Fig. 2 illustrates the 2D diagrams validating the docking protocol by re-docking the co-crystallized ligand in the active site. The re-docking validation step successfully reproduced the experimental binding pattern of the co-crystallized ligand, confirming the suitability of the adapted docking protocol for this study. The results for each target protein are as follows:

(1) 7YRZ (HCoV 229E main protease): the docking pose showed a small RMSD of 1.139 Å compared to the co-crystallized ligand, with an energy score of  $-28.97 \text{ kcal mol}^{-1}$ . The docking pose reproduced key interactions with active site hotspots (Cys144, Gln163, Glu165, His41, and Pro188).

(2) 2Q6F (IBV main protease): the docking yielded a small RMSD of 1.09 Å and an energy score of  $-25.21 \text{ kcal mol}^{-1}$ . It accurately reproduced binding interactions with key amino acids (Val188, Glu187, His41, Gly141, His162, His161, and Glu164).

(3) 6VGY (MERS 3CL protease): the docking resulted in an RMSD of 1.929 Å and an energy score of  $-17.46 \text{ kcal mol}^{-1}$ , with binding to key hotspots (Cys148, Glu169, Gln192, Gln167, His41, and His166).

(4) 6WUU (SARS-CoV-2 papain-like protease): the docking produced an RMSD of 1.929 Å and an energy score of  $-22.87 \text{ kcal mol}^{-1}$ , showing binding interactions with Asp164, Gly163, Gly271, Cys111, His272, and Tyr168.

These results demonstrate the reliability of the docking protocol across all four target proteins. After the validation step, three compounds were tested against the four targets and produced high scores with binding poses that are represented in Tables 1–3.

### In vitro results

**Cytotoxicity and inhibitory activity of hydroxyquinolinyl-pyrazole candidates against coronaviruses.** In this study, the antiviral activity of hydroxyquinolinyl-pyrazole derivatives was assessed against three coronaviruses: SARS-CoV-2, HCoV-229E, and MERS-CoV. The concentrations (conc.) ranged from 10 000  $\text{mg mL}^{-1}$  to 1  $\text{mg mL}^{-1}$ . Hydroxychloroquine was used as a positive control antiviral drug. The half-maximal cytotoxic concentration ( $\text{CC}_{50}$ ) values were determined, indicating the concentration at which 50% of cell viability was compromised.



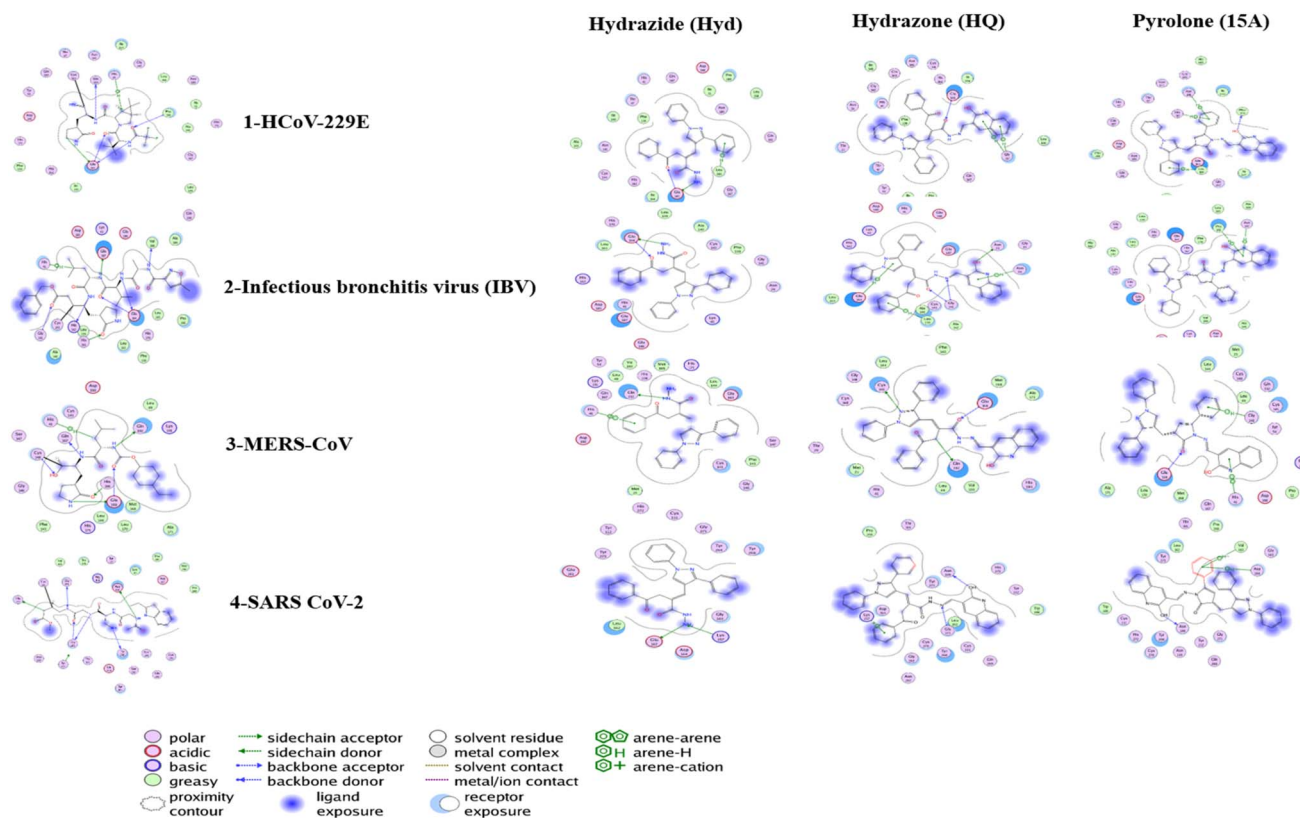


Fig. 2 2D Diagrams showing validation of docking protocol, by docking of the co-crystallized ligand in the active site.

Table 1 Scores of hydrazide (Hyd) with 229E, IBV, MERS, and SARS viruses

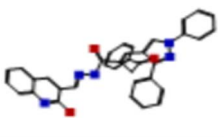
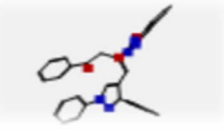
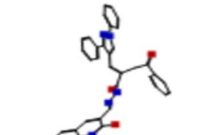
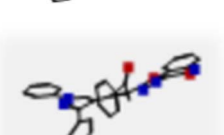
Structure	Virus	<i>S</i>	rmsd_refine	<i>E</i> _conf.	<i>E</i> _place	<i>E</i> _score1	<i>E</i> _refine	<i>E</i> _score2
	229E	-20.49	2.12	131.57	-81.40	-33.49	-20.22	-20.49
	IBV	-14.33	1.99	137.69	-43.44	-9.36	70.99	-14.33
	MERS	-21.31	1.27	128.01	-73.42	-25.59	15.99	-21.31
	SARS	-27.61	2.13	130.15	-83.94	-26.41	-40.95	-27.61

For all three viruses, the compounds exhibited varying degrees of inhibitory effects, as reflected by the half-maximal inhibitory concentration ( $IC_{50}$ ) values. Selectivity indices (SI) were

calculated by dividing  $CC_{50}$  by the corresponding  $IC_{50}$  for each virus. Notably, these compounds demonstrated promising



Table 2 Scores of hydrazone (HQ) with 229E, IBV, MERS, and SARS viruses

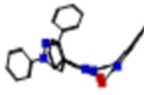
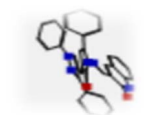
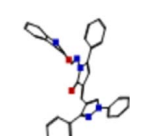
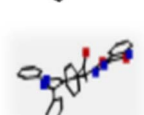
Structure	Virus	<i>S</i>	rmsd_refine	<i>E</i> _conf	<i>E</i> _place	<i>E</i> _score1	<i>E</i> _refine	<i>E</i> _score2
	229E	-20.42	2.83	118.66	-50.81	10.86	22.03	-21.96
	IBV	-17.23	2.54	121.39	-71.67	-21.39	-13.92	-17.23
	MERS	-22.09	2.91	120.56	-70.54	-24.94	-19.34	-22.09
	SARS	-26.53	2.35	119.87	-76.67	-27.98	-37.84	-26.53

selectivity against SARS-CoV-2 at lower concentrations, with increasing SI values (*cf.* Table 4 and Fig. 3).

Pyrazolylhydrazide (**Hyd**) exhibited a  $CC_{50}$  of 0.4913 mg mL<sup>-1</sup>, with notable inhibitory effects against SARS-CoV-2 ( $IC_{50}$ : 0.054 mg mL<sup>-1</sup>, SI: 9.09), MERS-CoV ( $IC_{50}$ : 0.23 mg mL<sup>-1</sup>, SI: 2.1), and HCoV-229E ( $IC_{50}$ : 0.0277 mg mL<sup>-1</sup>, SI: 17.7). Similarly, hydrazone **HQ** demonstrated promising results with a  $CC_{50}$  of

0.805 mg mL<sup>-1</sup> and significant inhibition against SARS-CoV-2 ( $IC_{50}$ : 0.052 mg mL<sup>-1</sup>, SI: 15.5), MERS-CoV ( $IC_{50}$ : 0.302 mg mL<sup>-1</sup>, SI: 2.7), and HCoV-229E ( $IC_{50}$ : 0.134 mg mL<sup>-1</sup>, SI: 6.0). In turn, pyrrolone **15A** exhibited potent antiviral activity and displayed higher cytotoxicity, necessitating further investigation. These findings underscore the potential of these derivatives as selective antiviral agents, particularly against SARS-CoV-2 and

Table 3 Scores of pyrrolone (15A) with 229E, IBV, MERS, and SARS viruses<sup>a</sup>

Structure	Virus	<i>S</i>	rmsd_refine	<i>E</i> _conf	<i>E</i> _place	<i>E</i> _score1	<i>E</i> _refine	<i>E</i> _score2
	229E	-25.75	3.95	158.57	-69.03	-20.80	-23.16	-25.75
	IBV	-19.65	2.56	157.27	-85.14	-26.71	-24.76	-19.65
	MERS	-20.16	1.62	178.04	-77.59	-10.42	40.05	-20.99
	SARS	-20.84	1.67	198.40	-3.40	-25.18	227.71	-20.13

<sup>a</sup> *S* (Score): the overall docking score (lower values indicate better binding). All energy values are in kcal mol<sup>-1</sup>. rmsd\_refine: root mean square deviation after refinement *E*\_conf: conformer energy. *E*\_place: placement energy *E*\_score1: initial scoring function energy. *E*\_refine: refinement energy *E*\_score2: final scoring function energy.



Table 4 Antiviral potency and selectivity of pyrazole derivatives against SARS-CoV-2, MERS-CoV, and HCoV-229E

Compounds	CC <sub>50</sub> (mg mL <sup>-1</sup> )	SARS-CoV-2		MERS-CoV		HCoV-229E	
		IC <sub>50</sub> (mg mL <sup>-1</sup> )	SI	IC <sub>50</sub> (mg mL <sup>-1</sup> )	SI	IC <sub>50</sub> (mg mL <sup>-1</sup> )	SI
Hydrazide (Hyd)	0.4913	0.054	9.09	0.23	2.1	0.0277	17.7
Hydrazone (HQ)	0.805	0.052	15.5	0.302	2.7	0.134	6.0
Pyrralone (15A)	65.362	0.158	413	0.0516	1266	0.0447	1462

HCoV-229E, providing valuable insights for future therapeutic development.

**In vitro mechanism of action results.** The results of screening for hydroxyquinoline-pyrazole derivatives as direct

antiviral agents, as well as IC<sub>50</sub> and protein docking studies, strongly suggest that these derivatives possess significant direct antiviral activity against SARS-CoV-2, MERS-CoV, and HCoV-229E. To validate and further elucidate these findings, we

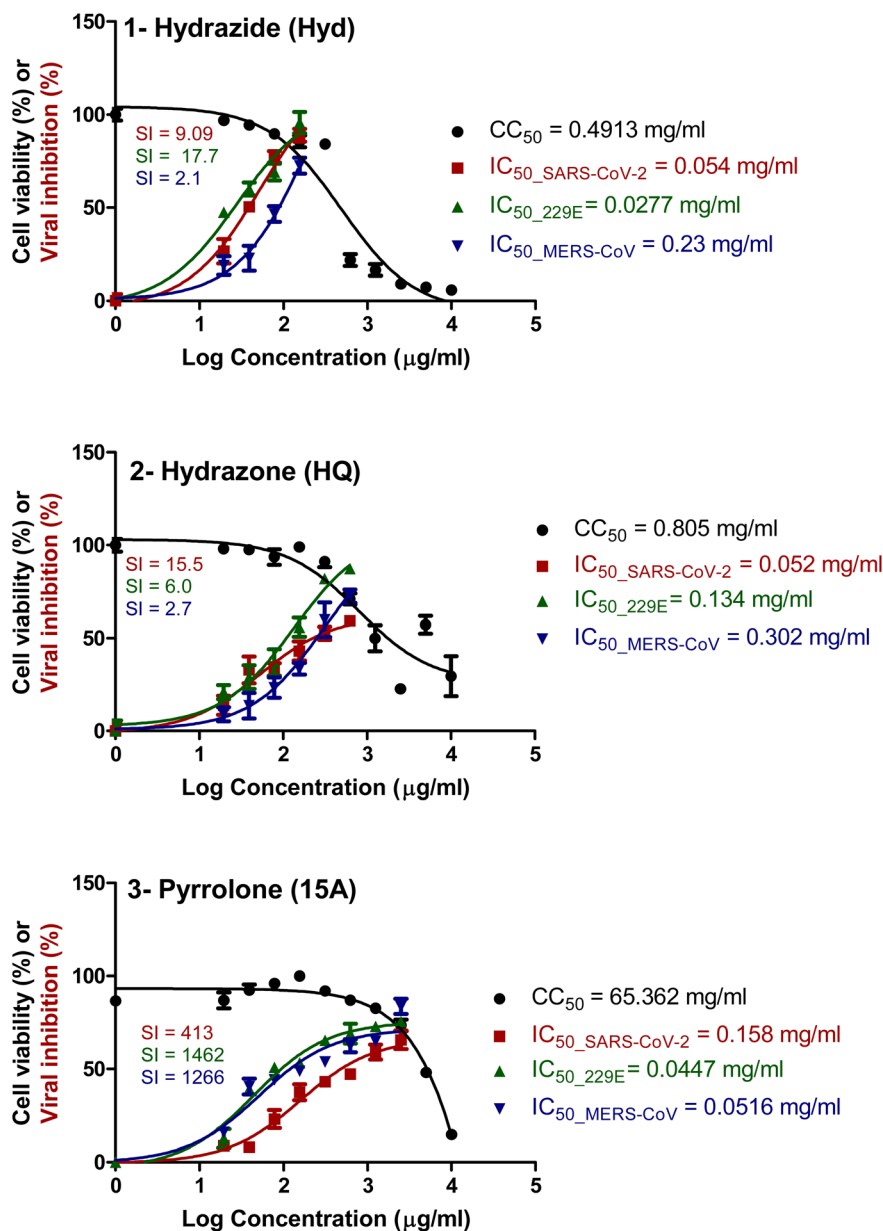


Fig. 3 Determination of CC<sub>50</sub> and IC<sub>50</sub> of hydrazide (Hyd), hydrazone (HQ) and pyrrolone (15A) in Vero E6 cells against SARS-CoV-2, MERS-CoV, and HCoV-229E. Values of CC<sub>50</sub> and IC<sub>50</sub> were calculated using non-linear regression analysis with Graph Pad Prism software (version 5.01).





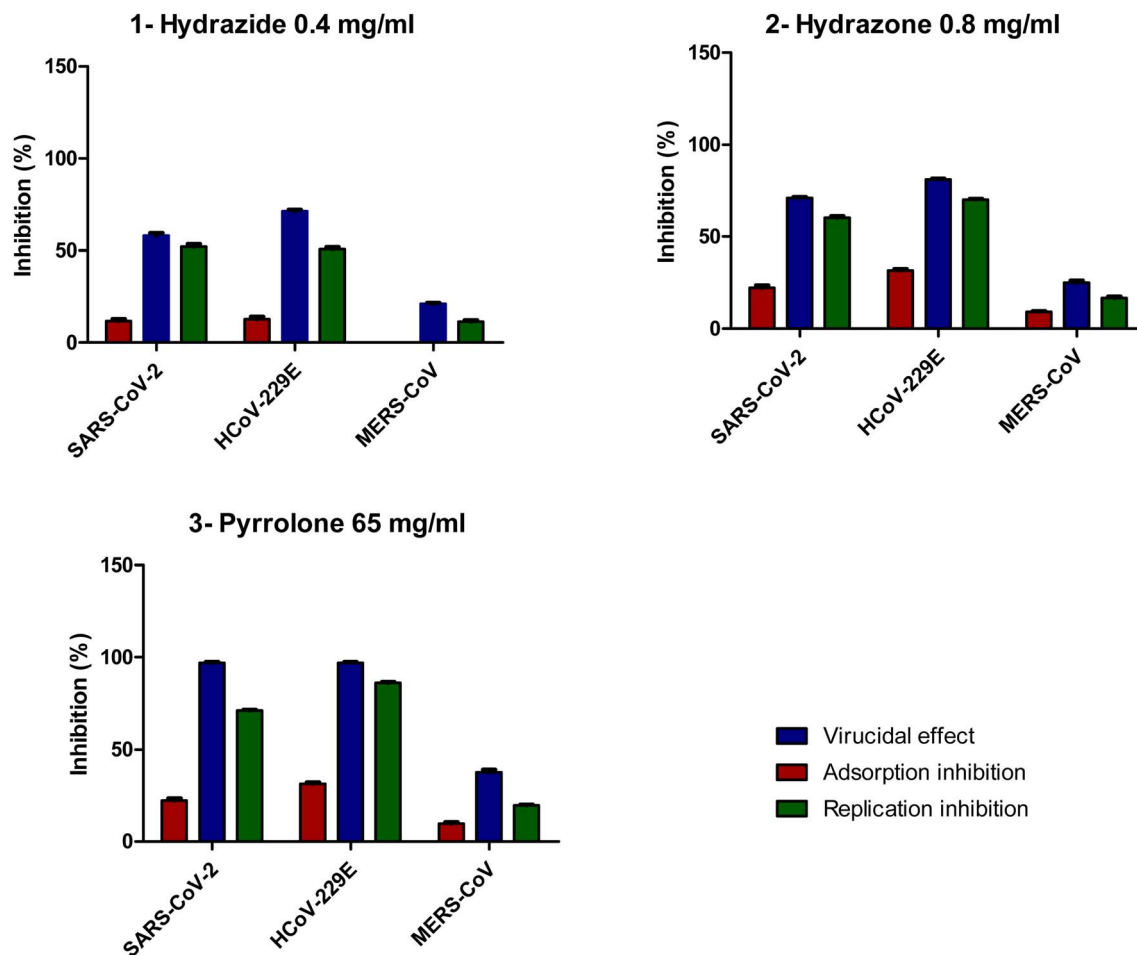


Fig. 4 Mode of action of hydroxyquinoline-pyrazole candidates against three coronaviruses on Vero-E6 cells, showing that pyrrolone reduced viral replication in different stages in viral replication cycle of the three tested coronaviruses.

conducted dose-dependent viral inhibition assays employing three distinct modes of action. The outcomes demonstrated that hydroxyquinoline-pyrazole candidates exhibited pronounced attenuation of coronaviruses through three distinct modes of action, as illustrated in Fig. 4.

The results indicate the percentage of inhibition observed for three different modes of action (adsorption inhibition, virucidal effect, and replication inhibition) against three coronaviruses (SARS-CoV-2, HCoV-229E, and MERS-CoV) at a concentration of  $0.4 \text{ mg mL}^{-1}$  of the tested compound (presumably hydrazone **Hyd**). These findings highlight the multifaceted antiviral mechanisms of the hydroxyquinoline-pyrazole derivatives, demonstrating their potential as broad-spectrum antiviral agents against various coronaviruses.

Adsorption inhibition, this measures the ability of the compound to prevent the virus from attaching to host cells. For SARS-CoV-2 and HCoV-229E, the inhibition percentages are 11.67%, and 12.76% indicating some level of effectiveness in preventing viral attachment. However, for MERS-CoV, the compound shows no significant adsorption inhibition.

Virucidal effect, that assesses the compound's ability to directly deactivate the virus. Notably, the compound

demonstrates substantial virucidal effects against all three viruses, with percentages ranging from 20% to 73%. This suggests that the compound is highly effective at directly neutralizing the viruses. Replication inhibition, this evaluates the compound's ability to hinder viral replication within host cells. The results show moderate to high inhibition percentages across all three viruses, ranging from 10% to 55%. This indicates that the compound is effective at impeding viral replication processes.

The hydrazone **HQ** exhibited significant adsorption inhibition with mean values of 20.67%, 31.67%, and 9.00% for SARS-CoV-2, HCoV-229E, and MERS-CoV, respectively. Regarding the virucidal effect, mean inhibition percentages were 71.33%, 81.00%, and 26.33% for SARS-CoV-2, HCoV-229E, and MERS-CoV, respectively. Furthermore, replication inhibition showed mean values of 60.33%, 70.00%, and 16.67% for SARS-CoV-2, HCoV-229E, and MERS-CoV, respectively.

These findings suggest that hydrazone **HQ** with  $0.8 \text{ mg mL}^{-1}$  concentration effectively attenuates the coronaviruses through adsorption inhibition, virucidal effect, and replication inhibition in a dose-dependent manner. Notably, HCoV-229E exhibits the highest susceptibility to the substance across all

mechanisms tested, followed by SARS-CoV-2, while MERS-CoV demonstrates comparatively lower susceptibility.

The results obtained for pyrrolone **15A** at a concentration of 65 mg mL<sup>-1</sup> demonstrate its inhibitory effects against SARS-CoV-2, HCoV-229E, and MERS-CoV across various mechanisms of action. Mean values were calculated to provide a comprehensive overview of the inhibitory activity. For adsorption inhibition, mean percentages were 19.67%, 31.33%, and 9.67% for SARS-CoV-2, HCoV-229E, and MERS-CoV, respectively. Notably, the virucidal effect was prominent, with mean inhibition percentages of 94.33%, 97.00%, and 37.67% for SARS-CoV-2, HCoV-229E, and MERS-CoV, respectively. Additionally, replication inhibition showed mean values of 70.33%, 85.33%, and 19.67% for SARS-CoV-2, HCoV-229E, and MERS-CoV, respectively. These results indicate that pyrrolone **15A** exhibits remarkably potent antiviral activity against HCoV-229E and SARS-CoV-2, while demonstrating relatively lower efficacy against MERS-CoV across all tested mechanisms of action.

## Discussion

This study aims at synthesizing new hydroxyquinoline-pyrazole systems and their antiviral efficacy on the recent SARS-CoV-2 and other coronaviruses such as MERS-CoV and HCoV-229E. The research topic seeks to determine the effectiveness of these compounds as antiviral agents for coronaviral diseases.

A synthesis of the target compounds, which are pyrazole-based quinoline derivatives, can be easily described. Looking for the efficient construction of hydrazone and pyrrolone, the authors reacted pyrazolylhydrazide with 2-chloro-3-formylquinoline under various reaction conditions. Thus, the synthetic strategy described here correlates with the new works devoted to the elaboration of new heterocyclic derivatives with antiviral activity. For instance, Seliem *et al.* described the synthesis of pyrazolothiazole conjugates to act as SARS-CoV-2 inhibitors with the view of advantage of pyrazole derived molecules in seeking coronavirus.<sup>13</sup>

The molecular docking study also helps in predicting the probable interactions which the synthesized compounds may have with the important viral targets. Concerning the choice of the appropriate protein targets for docking, an emphasis on the main protease and papain-like protease in coronaviruses adds importance to the outcome. The docking scores reveal a high level of compounds' binding to the viral proteins, and the poses indicate their possible interactions, which indicates their antiviral properties. This approach is in concordance with other computational studies conducted recently by Musa *et al.*, where they utilized molecular docking in order to establish phenylpyrazolone-1,2,3-triazole hybrids as good inhibitors of SARS-CoV-2 main protease.<sup>33</sup>

It could also be seen that the compounds had antiviral effects of retarding the viral replication of SARS-CoV-2, MERS-CoV, and HCoV-229E and establishing the compounds as possible antiviral agents. The implication of evaluating the CC<sub>50</sub> and IC<sub>50</sub> enables one to determine the toxicity of a compound towards cells as well as the effectiveness of the antiviral

compound. The obtained selectivity indices SI prove that the mentioned compounds enhance the selectivity toward SARS-CoV-2, mainly at relatively low concentrations. These outcomes correlate with research discussing the antiviral effect of heterocyclic compounds concerning coronaviruses. For instance, Kandinska *et al.* developed new tetrahydroisoquinoline hybrids containing other heterocyclic groups and compared their antiviral coronavirus potency.<sup>17</sup>

The inhibitory effects observed against several coronaviruses to support the broad-spectrum possibility of the synthesized candidates. This is extremely relevant considering that the threat of new Covid-19 variants is still present and that there is a need for universal antiviral agents. The multi-target approach that is targeting various phases of virus reproduction meets contemporary approaches to the development of drugs used to combat viruses. For example, Chang *et al.* have very recently published cytotoxic hexadepsipeptides and anti-coronaviral 4-hydroxy-2-pyridones from an endophytic *Fusarium* sp. Amalgamating the data presented in the works under analysis and the general information concerning the oligomerization of pyrroles, it is possible to assert that the search for antiviral compounds with novel chemical scaffolds will remain one of the most effective strategies for further research.<sup>34</sup>

The positive results indicated in this work call for additional future research, which should encompass *in vivo* evaluation of the agent's effectiveness and determination of the toxic effects of the compound. Moreover, structural modifications of the synthesized compounds could be involving an attempt to improve the antiviral activity along with selectivity. Understanding the specific mechanisms by which these compounds work against the viruses would further explain their use in the treatment of coronaviruses.

Besides, the prediction of ADME properties using SwissADME offers information on the likeliness of the compounds as drugs and information on the potential bioavailability. This approach typically assumes a greater significance in the course of the initial drug discovery phase, especially as exposed by recent studies, for example, *in silico* ADME/pharmacokinetics predictions were applied to estimate the property of 5-substituted 1*H*-tetrazole and benzoquinoline derivatives.<sup>35,36</sup>

Therefore, this work should be regarded as the investigation of the existing literature in the field of the development of potential antiviral substances against coronaviruses. The use of synthetic chemistry, molecular modeling and biological evaluation enables for a systematic approach for screening of active molecules. The findings signify the potential use of hydroxyquinoline-pyrazole derivatives with the antiviral activity across different coronaviruses and provide the direction for further experimental studies with the view of creating means for the coronaviral infections treatment.

## Modeling pharmacokinetics

The ADME (absorption, distribution, metabolism, and excretion) properties of the potent substances, which comprise their physicochemical characteristics, lipophilicity, and drug-likeness, have been predicted by SwissADME free web tool to



lower the time of picking substances from an huge collection of substances in the primary phases of drug finding, biological possessions, and development for an operative drug.<sup>37</sup> The hydrazide **Hyd**, hydrazone **HQ**, and pyrrolone **15A** were found to obey with Lipinski's rule of five with a total polar surface area (TPSA) of 90.01, 109.47, and 83.61 Å<sup>2</sup>, respectively (*cf.* Table S1 and Fig. S1–S3 in ESI†).

Also, these substances displayed appropriate physicochemical properties, which were assessed through the following six parameters: size, lipophilicity, polarity, unsaturation, insolubility, and flexibility. Regarding the absorption property, they demonstrated gastrointestinal tract (GIT) absorption owing to their being in the BOILED-EGG chart white area (Fig. S4 in ESI†). The compounds demonstrated favorable lipophilicity profiles, as indicated by their consensus log  $P_{o/w}$  values of 3.36, 5.50, and 5.83 for hydrazide (**Hyd**), hydrazone (**HQ**), and pyrrolone (**15A**), respectively. The bioavailability radar chart revealed promising oral bioavailability for both **Hyd** and **HQ**, with a value of 0.55. All three compounds (hydrazide **Hyd**, hydrazone **HQ**, and pyrrolone **15A**) were fully encompassed within the pink area of the chart, suggesting good predicted oral bioavailability. This analysis considered key physicochemical properties including lipophilicity, polarity, molecular size, solubility, flexibility, and saturation. The results indicate that these compounds possess a balanced profile of these properties, which is favorable for oral drug candidates.

Compound (**Hyd**) revealed a high GIT absorption while the others showed low GIT absorption. Their skin permeation (log  $K_p$ ) constraints were  $-6.18$ ,  $-5.27$ , and  $-4.67$  cm s<sup>-1</sup>, which given the bioactive substrates easy going to retrieve through skin. Furthermore, their cytochrome P450 isoenzymes, which accomplish a substantial role in medicines biotransformation through O-type oxidation processes, have also been anticipated. Otherwise, it is expected to access the blood–brain barrier (existed inside chart yellow area). The compounds colored red in Fig. S4† did not enter the substrate area for P-glycoprotein. A major efflux transporter is P-gp, which is capable of limiting drug oral absorption and brain penetration, so normally the nonsubstrate status is favorable for bioavailability upon oral administration and for CNS penetration.

On the other side, in terms of compliance with Lipinski's rule of five, which predicts bioavailability after oral administration, hydrazide (**Hyd**) did not reveal any violations, and neither did hydrazone **HQ**. In the case of pyrrolone (**15A**), it had one violation, probably because of its a bit higher log  $P$  value of 5.83, which was a little over the recommended limit of 5. At the same time, all three compounds (**Hyd**, **HQ**, and **15A**) revealed very favorable drug-like properties and were predicted to have good oral bioavailability. The log  $P$  values for **Hyd** and **HQ** were 3.36 and 5.50, falling within or very near to the ideal range of 1.35 to 5, likely to have good oral absorption. Although compound **15A** presented higher lipophilicity, which may add advantages regarding membrane permeability, it could somewhat affect aqueous solubility. These *in silico* predictions taken together indicate that the physicochemical profile of the synthesized compounds is compatible with oral drug-likeness

and bioavailability; the profiles of **Hyd** and **HQ** were very promising.

## Conclusion

This work fills the research gap of the design, synthesis, and antiviral activity of hydroxyquinoline-pyrazole derivatives against various coronaviruses. Thus, the synergistic use of *in silico* molecular docking studies and *in vitro* antiviral assays gives a full picture of the compounds' perspective as antiviral agents.

Key findings from this research include:

(1) New hydroxyquinoline-pyrazole derivatives; hydrazide (**Hyd**), hydrazone (**HQ**), and pyrrolone (**15A**) were synthesized and characterized.

(2) Shown to have ambivalent activity against SARS-CoV-2, as well as MERS-CoV and HCoV229E with selectivity indices, suggesting potentially selective antiviral agents.

(3) Learning of four possibilities of action, namely, adsorption inhibition, virucidal effectivity, replication hindrance, and encapsidation interference, implying that the physical chemical had a good potential of acting against a myriad of viruses.

(4) drug likeness and oral bioavailability of the synthesized compound have been found to be favorable based on the ADME prediction models.

These findings have broader implications for antiviral drug discovery and development:

(1) The present work represents a novel example of using congeneric series of hydroxyquinoline and pyrazole derived compounds to improve antiviral effect and specificity to a group of coronaviruses.

(2) The compounds discussed above have multiple target activity profiles, which is in parallel with the current trends in the antiviral drugs design, which might have certain advantages over single target ones.

(3) The conceptualization and the assessment that prioritized in this study are fast, and the layout of the study can be used as a blueprint of sorts for an accelerated antiviral drug development when new viral threats emerge.

Future research directions stemming from this work include:

(1) The extension of lead compounds aiming at improving the antiviral efficacy and selectivity.

(2) Further *in vitro* studies to determine the theoretical working of these compounds towards the coronavirus.

(3) Further testing of these compounds with the spectrum of viruses other to see their potentials as broad-spectrum antiviral agents.

(4) *In vivo* efficacy and toxicity studies to evaluate the anti-fungal activity and safety of the above compounds.

(5) Evaluation of the possibilities of the combined application with other antiviral drugs.

(6) The rational and knowledge-based design of new antiviral derivatives using the hydroxyquinoline-pyrazole template through the understanding of the SAR rules.

Therefore, this study advances knowledge that could be used to progress subsequent works aimed at finding the appropriate



treatments for coronaviral infections. The positive results which have been achieved with these hydroxyquinoline-pyrazole derivatives, serves as aspect of curiosity about these compounds as a fresh stage of antiviral brokers. Further research and enhancement of these compounds could go a long way to improve on current strategies dealing with present and future coronavirus pandemics in the world healthcare facilities.

## Ethical statement

This study was approved by the Institutional Animal Care and Use Committee at Agricultural Research Center (Approval code: ARC, CLEVB, 27, 24) and was performed in accordance with the guidelines of the National Institute of Health (NIH). All methods are reported in accordance with ARRIVE guidelines.

## Data availability

All data generated or analyzed during this study are included in this published article and its ESI files.†

## Conflicts of interest

The authors declare no competing interests.

## References

- 1 C. Liu, *et al.*, Research and Development on Therapeutic Agents and Vaccines for COVID-19 and Related Human Coronavirus Diseases, *ACS Cent. Sci.*, 2020, **6**(3), 315–331.
- 2 A. Dutta, A. Roy, L. Roy, S. Chattopadhyay and S. Chatterjee, Immune response and possible therapeutics in COVID-19, *RSC Adv.*, 2021, **11**, 960–977.
- 3 Z. B. Milanovic, *et al.*, Inhibitory activity of quercetin, its metabolite, and standard antiviral drugs towards enzymes essential for SARS-CoV-2: the role of acid–base equilibria, *RSC Adv.*, 2021, **11**, 2838–2847.
- 4 U. Farwa and M. A. Raza, Heterocyclic compounds as a magic bullet for diabetes mellitus: a review, *RSC Adv.*, 2022, **12**, 22951–22973.
- 5 D. A. Milenković, D. S. Dimić, E. H. Avdovićac and Z. S. Marković, Several coumarin derivatives and their Pd(ii) complexes as potential inhibitors of the main protease of SARS-CoV-2, an *in silico* approach, *RSC Adv.*, 2020, **10**, 35099–35108.
- 6 J. Branković, *et al.*, Pyrazolone-type compounds: synthesis and *in silico* assessment of antiviral potential against key viral proteins of SARS-CoV-2, *RSC Adv.*, 2022, **12**, 16054–16070.
- 7 S. K. Ramadan, S. S. Shaban and A. I. Hashem, Facile and expedient synthesis and anti-proliferative activity of diversely pyrrolones bearing 1,3-diphenylpyrazole moiety, *Synth. Commun.*, 2020, **50**(2), 185–196.
- 8 A. R. Morsy, S. K. Ramadan and M. M. Elsafty, Synthesis and antiviral activity of some pyrrolonyl substituted heterocycles as additives to enhance inactivated Newcastle disease vaccine, *Med. Chem. Res.*, 2020, **29**, 979–988.
- 9 S. K. Rampadan, *et al.*, Some pyrimidohexahydroquinoline candidates: synthesis, DFT, cytotoxic activity evaluation, molecular docking, and *in silico* studies, *RSC Adv.*, 2024, **14**(23), 16584–16599.
- 10 B. Y. Li, *et al.*, Quinoline, with the active site of 8-hydroxyl, efficiently inhibits *Micropterus salmoides* rhabdovirus (MSRV) infection *in vitro* and *in vivo*, *J. Fish Dis.*, 2022, **45**(6), 895–905.
- 11 S. K. Ramadan, H. S. Abd-Rabboh, N. M. Gad, W. S. I. Abou-Elmagd and D. Haneen, Synthesis and characterization of some chitosan-quinoline nanocomposites as potential insecticidal agents, *Polycyclic Aromatic Compounds*, 2023, **43**(8), 7013–7026.
- 12 H. A. Saadeh, K. A. Sweidan and M. S. Mubarak, Recent advances in the synthesis and biological activity of 8-hydroxyquinolines, *Molecules*, 2020, **25**(18), 4321.
- 13 A. F. Seliem, Synthesis and Virtual Screening of Pyrazolothiazole Conjugates as Promising SARS-CoV-2 Inhibitors, *ChemistrySelect*, 2023, **8**(19), e202300605.
- 14 A. S. Elgubbi, E. A. E. El-Helw, A. Y. Alzahrani and S. K. Ramadan, Synthesis, computational chemical study, antiproliferative activity screening, and molecular docking of some thiophene-based oxadiazole, triazole, and thiazolidinone derivatives, *RSC Adv.*, 2024, **14**(9), 5926–5940.
- 15 A. M. Abdelrahman, A. A. Fahmi, S. A. Rizk and E. A. E. El-Helw, Synthesis, DFT and Antitumor Activity Screening of Some New Heterocycles Derived from 2,2'-(2-(1,3-Diphenyl-1H-pyrazol-4-yl)ethene-1,1-diyl)bis(4H-benzo[d][1,3]oxazin-4-one), *Polycyclic Aromatic Compounds*, 2023, **43**(1), 721–739.
- 16 M. M. Kaddah, A. A. Fahmi, M. M. Kamel, S. A. Rizk and S. K. Ramadan, Rodenticidal Activity of Some Quinoline-Based Heterocycles Derived from Hydrazide-Hydrazone Derivative, *Polycyclic Aromatic Compounds*, 2023, **43**(5), 4231–4241.
- 17 M. I. Kandinska, *et al.*, Synthesis of Novel 1-Oxo-2,3,4-trisubstituted Tetrahydroisoquinoline Derivatives, Bearing Other Heterocyclic Moieties and Comparative Preliminary Study of Anti-Coronavirus Activity of Selected Compounds, *Molecules*, 2023, **28**(3), 1495.
- 18 A. Kandeil, *et al.*, Middle East respiratory syndrome coronavirus (MERS-CoV) in dromedary camels in Africa and Middle East, *Viruses*, 2019, **11**(8), 717.
- 19 O. Kutkat, *et al.*, Robust antiviral activity of commonly prescribed antidepressants against emerging coronaviruses: *in vitro* and *in silico* drug repurposing studies, *Sci. Rep.*, 2022, **12**(1), 12920.
- 20 M. R. Gomaa, *et al.*, Incidence, household transmission, and neutralizing antibody seroprevalence of Coronavirus Disease 2019 in Egypt: Results of a community-based cohort, *PLoS Pathog.*, 2021, **17**(3), e1009413.
- 21 L. J. Reed and H. Muench, A simple method of estimating fifty per cent endpoints, *Am. J. Epidemiol.*, 1938, **27**(3), 493–497.
- 22 M. Feoktistova, P. Geserick and M. Leverkus, Crystal violet assay for determining viability of cultured cells, *Cold Spring Harb. Protoc.*, 2016, **2016**(4), 343–346.



- 23 T. Mosmann, Rapid colorimetric assay for cellular growth and survival: application to proliferation and cytotoxicity assays, *J. Immunol. Methods*, 1983, **65**(1–2), 55–63.
- 24 A. Mostafa, *et al.*, FDA-approved drugs with potent in vitro antiviral activity against severe acute respiratory syndrome coronavirus 2, *Pharmaceuticals*, 2020, **13**(12), 443.
- 25 A. Kandeil, *et al.*, Coding-complete genome sequences of two SARS-CoV-2 isolates from Egypt, *Microbiol. Resour. Announce.*, 2020, **9**(22), 004899.
- 26 F. G. Hayden, K. Cote and R. G. Douglas-Jr, Plaque inhibition assay for drug susceptibility testing of influenza viruses, *Antimicrob. Agents Chemother.*, 1980, **17**(5), 865–870.
- 27 M. Kuo, M. H. Browning and M. L. Penner, Do lessons in nature boost subsequent classroom engagement? Refueling students in flight, *Front. Psychol.*, 2018, **8**, 2253.
- 28 M. Zhang, T. Tanaka and M. Ikura, Calcium-induced conformational transition revealed by the solution structure of apo calmodulin, *Nat. Struct. Biol.*, 1995, **2**(9), 758–767.
- 29 W. S. I. Abou-Elmagd, *et al.*, Synthesis and anti H5N1 activities of some pyrazolyl substituted N-heterocycles, *Nat. Sci.*, 2016, **14**(9), 115.
- 30 E. A. E. El-Helw, A. R. Morsy and A. I. Hashem, Evaluation of some new heterocycles bearing 2-oxoquinolyl moiety as immunomodulator against highly pathogenic avian influenza virus (H5N8), *J. Heterocycl. Chem.*, 2021, **58**(4), 1003–1014.
- 31 S. K. Ramadan, *et al.*, Synthesis, SAR studies, and insecticidal activities of certain N-heterocycles derived from 3-((2-chloroquinolin-3-yl)methylene)-5-phenylfuran-2(3H)-one against *Culex pipiens* L. larvae, *RSC Adv.*, 2022, **12**(22), 13628–13638.
- 32 M. M. Kaddah, *et al.*, Synthesis and biological activity on IBD virus of diverse heterocyclic systems derived from 2-cyano-N'-((2-oxo-1,2-dihydroquinolin-3-yl)methylene)acetohydrazide, *Synth. Commun.*, 2021, **51**(22), 3366–3378.
- 33 A. Musa, *et al.*, Phenylpyrazolone-1,2,3-triazole hybrids as potent antiviral agents with promising SARS-CoV-2 main protease inhibition potential, *Pharmaceuticals*, 2023, **16**(3), 463.
- 34 S. Chang, *et al.*, Nocaviogua A and B: two lipolanthines from root-nodule-associated *Nocardia* sp, *Front. Chem.*, 2023, **11**, 1233938.
- 35 A. El-Sewedy, *et al.*, One-pot synthesis, computational chemical study, molecular docking, biological study, and in silico prediction ADME/pharmacokinetics properties of 5-substituted 1 H-tetrazole derivatives, *Sci. Rep.*, 2023, **13**(1), 17869.
- 36 E. A. E. El-Helw, M. Asran, M. E. Azab, M. H. Helal, A. Y. Alzahrani and S. K. Ramadan, Synthesis and in silico studies of certain benzo[f]quinoline-based heterocycles as antitumor agents, *Sci. Rep.*, 2024, **14**, 15522.
- 37 C. A. Lipinski, Lead-and drug-like compounds: the rule-of-five revolution, *Drug Discovery Today: Technol.*, 2004, **1**(4), 337–341.

